Journal of Metals, Materials and Minerals, 33(4), 1779, 2023

Improvement of specific capacity of lithium iron phosphate battery by increasing the surface area and electrical conductivity of cathode electrode using graphene foam

Phurida KOKMAT[1], Patiphat MATSAYAMAT[2], Kunaree WONGRACH[2], Piyaporn SURINLERT[3,4], and Akkawat RUAMMAITREE[1,4,*]

[1] *Department of Physics, Faculty of Science and Technology, Thammasat University, Phahon Yothin, Khlong Luang, Pathum Thani 12120, Thailand*
[2] *Department of Physics, Faculty of Science, Burapha University, Long-Hard Bangsaen, Muang, Chonburi 20131, Thailand*
[3] *Chulabhorn International College of Medicine, Thammasat University, Phahon Yothin, Khlong Luang, Pathum Thani 12120, Thailand*
[4] *Thammasat University Research Unit in Synthesis and Applications of Graphene, Thammasat University, Phahon Yothin, Khlong Luang, Pathum Thani 12120, Thailand*

***Corresponding author e-mail:** akkawat@tu.ac.th

Received date:
30 June 2023
Revised date
11 July 2023
Accepted date:
11 July 2023

Keywords:
Graphene foam;
Lithium iron phosphate;
Lithium-ion battery;
Chemical vapor deposition

Abstract

Lithium iron phosphate (LFP) is widely used as an active material in a cathode electrode for lithium-ion batteries (LIBs). LFP has many remarkable properties such as high working voltage and excellent thermal stability. However, it suffers with slow ion diffusion and low electrical conductivity. Graphene foam has many outstanding properties such as large surface area and great electrical conductivity. These properties are suitable for improving the cathode electrode. In this work, the graphene foam was synthesized by chemical vapor deposition. The cathode electrode was prepared by dropping the LFP on the graphene foam. We found that the specific capacity of battery which contained the LFP between the anode and the graphene foam (LFP/GF) was 23.1 $mAh{\cdot}g^{-1}$ at 3C, while the specific capacity of battery which contained the graphene foam between the anode and the LFP (GF/LFP) was 112.6 $mAh{\cdot}g^{-1}$ at 3C. The diffusion coefficients of Li^+ of GF/LFP was 9.1 times higher than that of LFP/GF. The specific capacity of GF/LFP was higher than that of LFP/GF at high current density due to the high ion transfer rate which arises from the graphene foam.

1. Introduction

A lithium-ion battery is widely used in many electronic devices because of high energy density and long-life cycle. The life and performance of the lithium-ion battery mainly depend on the three significant parts, namely cathode electrode, anode electrode and electrolyte. For improvement of the cathode electrode, many materials such as lithium iron phosphate ($LiFePO_4$), lithium cobalt oxide ($LiCoO_2$) and lithium manganese oxide ($LiMn_2O_4$) are used as active material in the cathode electrode [1]. $LiFePO_4$ or LFP is widely utilized as the active material in the cathode electrode in lithium-ion battery because it has high specific capacity (170 $mAh{\cdot}g^{-1}$), thermal stability [2], flat potentials at ~3.4 V during charge/discharge. However, the LFP has poor electrical conductivity [3] and slow ion diffusion. To deal with these problems, addition of conductive material with high surface area on the LFP is needed to increase the electrical conductivity and ion diffusion speed. There are many researchers trying to improve the electrochemical performance of LFP battery. Raj *et al*. coated carbon on LFP to enhance the discharge capacity of LFP battery up to 148.2 $mAh{\cdot}g^{-1}$ at 0.1 C. [4], Ni *et al*. improved the capacity delivery and cycle performance by metal doping [5], Tian reduced the charge transfer resistance using the graphene-coated LFP [6], and Ji *et al*. increased the surface area and electrical conductivity of electrode using three-dimensional porous graphite foam to enhance the specific capacity [7].

Graphene is a two-dimensional honeycomb crystal of carbon atoms. Graphene has many excellent properties such as high carrier mobility [8], superior thermal conductivity [9], linear dispersion at the K-point [10-12], large specific surface area [13] and extremely high intrinsic strength [14]. Graphene foam is a three-dimensional network of graphene therefore the surface area of graphene foam is much higher than that of graphene. Although graphene can be synthesized by various methods such as annealing SiC [15-17], Calcination at high temperatures [18,19] and chemical vapor deposition (CVD) [20,21]. However, the CVD is the most facile and low-cost method for synthesis of graphene foam. The utilization of graphene foam as a current collector has attracted attention from researchers because the graphene foam has high surface area and great electrical conductivity resulting in the specific capacity increases [22].

In this study, the graphene foam is prepared by CVD method using nickel foam as a metal catalyst. The structure of graphene foam is analyzed using X-ray diffraction (XRD) and Raman spectroscopy. In addition, the specific capacities of LFP cathode using aluminum foil and graphene foam as current collectors are investigated. Besides, the assemblies of cathode electrode of LFP and graphene foam are studied.

2. Experimental

2.1 Material

Nickel foam (99.99% purity) was purchased from Xiamen Lith Machine Limited, China. LFP powder, lithium foil and super P carbon black powder were bought from Xiamen Tob New Energy Technology Co., Ltd, China. Polyvinylidene fluoride (PVDF) and electrolyte were purchased from Sigma-Aldrich.

2.2 Preparation of Graphene foam

A nickel foam sheet was cleaned two times in acetone by ultrasonic sonication for 5 min. After that, the nickel foam was put in a quartz tube of CVD furnace. The air was evacuated from the quartz tube until the pressure reached ~10^{-3} torr. Then, the nickel foam was heated at 800°C followed by introducing acetylene gas with a flow rate of 10 sccm for 30 min in the quartz tube. Afterward the acetylene gas was stopped, and the sample was rapidly cooled down to room temperature. After that, the sample was cut into circle with a diameter of 1.6 cm. Finally, the sample was immersed in $FeCl_3$ and HCl to remove the nickel from the sample.

2.3 Preparation of the cathode electrode

Firstly, LFP, super P carbon black powder and PVDF were mixed (a weight ratio of 75:15:10) in N-methyl-2-pyrrolidone and stirred by the magnetic stirrer for 12 h. The slurry was dropped on the graphene foam and dried in the oven at 110°C for 24 h. The LFP on graphene electrode was retrieved. For the comparison, the cathode electrode using aluminum foil as a current collector was prepared by coating the slurry on the aluminum foil using the doctor blade method followed by drying in the oven at 110°C for 24 h.

2.4 Characterization

The crystalline structure of graphene foam was analyzed by XRD using a benchtop X-ray powder diffractometer (Bruker) with Cu-Ka radiation (λ=0.154184 nm). The Raman measurement was carried out at room temperature using a Horiba with 532 nm laser. Field-emission scanning electron microscope (Fe-SEM) was conducted by Hitachi UHR Fe-SEM SU8010 with an incident beam of 20 kV.

2.5 Electrochemical measurement

The graphene foam electrode was transferred into an argon-filled glove box for coil cell assembly (CR2032). The lithium foil and polypropylene membrane (Celegard 2400) were used as anode and separator, respectively. Lithium hexafluorophosphate solution in ethylene carbonate and dimethyl carbonate, 1.0 M $LiPF_6$ in EC/DMC =50/50(v/v), was utilized as the electrolyte. The cyclic voltammetry (CV) and DC charge/discharge were performed within the voltage window from 2.5 V to 4.2 V. The electrochemical impedance spectroscopy (EIS) was examined in a frequency range of 0.1 Hz to 1 MHz at room temperature.

3. Results and discussion

The structure of graphene foam was studied by XRD. The XRD pattern of graphene (Figure 1(a)) displayed the diffraction peak at 25.8° which corresponded to the (002) plane of graphene. The interlayer spacing of graphene can be determine using the Bragg's Equation [16].

$$2d\sin\theta = n\lambda \quad (1)$$

where d is an interlayer spacing. θ is an angle between the incident beam and the graphene surface. l is a wavelength of the incident X-ray beam. n is a diffraction order. Therefore, the presence of diffraction peak of graphene at 25.8° revealed that the interlayer spacing of the graphene was 0.345 nm. Besides, the XRD pattern showed the shoulder peaks at ~25° and 26.5° which corresponded to the interlayer spacings of 0.356 nm and 0.336 nm, respectively. The presence of shoulder peaks indicated the interlayer spacings of the graphene foam was not uniform. In general, the stacking pattern of graphene is AB stacking which contains the interlayer spacing of 0.335 nm. The interlayer spacings of the graphene foam of 0.345 nm and 0.356 nm were much larger than that of the AB stacked graphene implying some parts of the graphene foam contained turbostratic stacked graphene.

The Raman spectrum which measured on the surface of the graphene foam (Figure 1(b)) exhibited the significant peaks of D band, G band and 2D band at 1346 cm^{-1}, 1581 cm^{-1} and 2698 cm^{-1}, respectively. The D band arises from the sp^2-hybridized disordered carbon materials [23]. G band originates from the bond stretching between pairs of sp^2 carbon atoms [24]. The 2D band is a second-order mode of the D band. In addition, the intensity ratio of D peak and G peak (I_D/I_G) of the graphene foam was 0.0326. The I_D/I_G was utilized to estimate the crystallite size of graphene (L_a) using the following equation [25].

$$L_a(nm) = \left(2.4 \times 10^{-10}\right) \lambda_{laser}^4 \left(\frac{I_D}{I_G}\right)^{-1} \quad (2)$$

where, l_{laser} is the wavelength of incident laser (532 nm). The result revealed the crystallite size of graphene was 590 nm.

Turbostratic stacked graphene is multilayer graphene which has no interlayer interaction. Therefore, the electronic properties, such as the linear dispersion and carrier mobilities, similar to those of mono-layer graphene. Generally, the Raman spectrum of turbostratic graphene contains a peak of iTALO$^-$ mode at ~1850 cm^{-1}. The iTALO$^-$ mode arises from a combination of in-plane transverse acoustic (iTA) and the longitudinal optic (LO) phonons [26,27]. However, the Raman spectrum which measured on the surface of the graphene foam (Figure 1(b) inset) displayed no iTALO$^-$ peak at ~1850 cm^{-1} implying that the stacking type of graphene on the surface of the graphene foam was AB stacking. As the results of XRD and Raman, it can be concluded that the graphene foam consisted of AB stacked graphene outside and turbostratic stacked graphene inside. SEM images of the graphene foam (Figure 2) exhibited the 3D-network structure with high porosity leading to the high specific surface area.

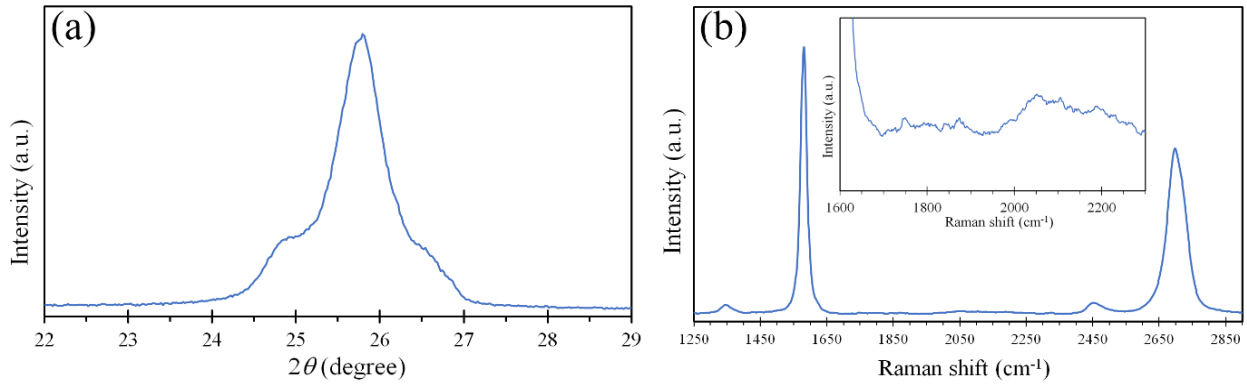

Figure 1. (a) XRD patterns of graphene foam, (b) Raman spectrum of graphene foam and Inset Magnified Raman spectrum of graphene foam in the range between 1600 cm^{-1} to 2300 cm^{-1}.

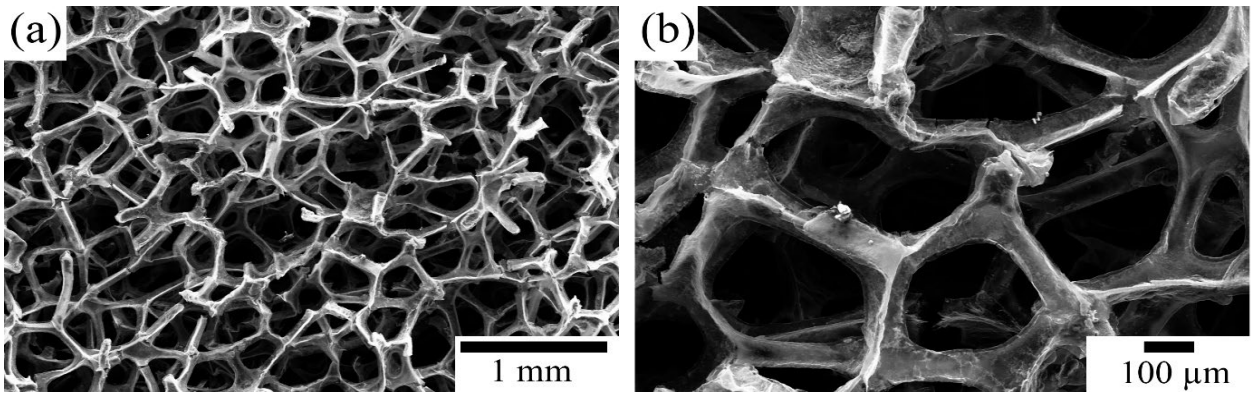

Figure 2. (a) SEM image of the graphene foam and (b) the magnified SEM image of (a).

For preparation of cathode electrodes, the slurry, which contains LFP, super P carbon black and PVDF, was dropped on a graphene foam disk with a diameter of ~16 mm (Figure 3(a)). The loading density of LFP is ~2.4 $mg{\cdot}cm^{-2}$. SEM image (Figure 3(b)) and EDX elemental distribution maps for oxygen, phosphorus, and iron (Figure 3(c-e)) confirmed the presence of LFP on the graphene foam surface. After that the samples were transferred to the argon-filled glove box for coil cell assembly. Figure 4 displays the three types of coin cell assemblies. Firstly, the LFP was between the separator sheet and the graphene foam. Secondly, the graphene foam was between the separator sheet and the LFP. Thirdly, the LFP was between the separator sheet and the aluminum foil. These three samples were designated as LFP/GF, GF/LFP and LFP/Al, respectively.

Figure 5(a) shows charge and discharge performances of LFP/Al, LFP/GF and GF/LFP at 0.1C revealing the flat plateau of discharge potential at ~3.4 V for the LFP/GF and GF/LFP, and ~3.3 V for LFP/Al. The Coulombic efficiencies of LFP/Al, LFP/GF and GF/LFP are 82.2%, 92.1% and 91.4%, respectively. Besides, the specific capacities of LFP/Al, LFP/GF and GF/LFP at 0.1C are 98 $mAh{\cdot}g^{-1}$, 155.2 $mAh{\cdot}g^{-1}$ and 155.5 $mAh{\cdot}g^{-1}$, respectively. The specific capacities of LFP/GF and GF/LFP are much higher than that of LFP/Al. This is attributed to the high surface area and great electrical conductivity of the graphene foam.

Figure 5(b-c) exhibit rate capabilities of LFP/GF and GF/LFP, respectively, at current densities from 0.1C to 5C for 5 cycles each. The specific capacities of both LFP/GF and GF/LFP decreased when the current density increased, especially at the current density of 5C, the specific capacities reduced more than 60%. The reduction of specific capacity with increment of current density due to the fact that the ions in the electrode and the electrolyte is not fast enough for transferring across the electrode/electrolyte interface and distributing to reach equilibrium [28]. However, these specific capacities were restored after decreasing the current density to 0.1C. Figure 5(d) shows a relationship between the average specific capacity and the discharge rate of LFP/GF and GF/LFP. The specific capacities of both LFP/GF and GF/LFP were similar at low current density. However, the specific capacity of LFP/GF becames much lower than that of GF/LFP at high current density (3C and 5C). The drastic reduction of specific capacity of LFP/GF at high current density arises from the low surface area and electrical conductivity of LFP resulting in low transfer rate of ions at high current density. On the other hand, in the case of GF/LFP, the graphene foam, which has high surface area and great electrical conductivity, connected directly with the electrolyte therefore the transfer rate of ions between the cathode electrode and electrolyte is much higher than that of LFP/GF. In order to investigate the cycling stability of GF/LFP, the GF/LFP was cycled at 3C for 100 cycles as shown in Figure 5(e). The discharge specific capacity increased from 109 $mAh{\cdot}g^{-1}$ to 127 $mAh{\cdot}g^{-1}$. The cycling performance also showed the discharge specific capacity of GF/LFP fluctuated at cycle 39^{th} and 62^{th}. In addition, the Coulombic efficiency increased from 97.34% to 99.45% after 100 cycles. Figure 5(f) exhibits CV curves of LFP/GF and GF/LFP. The CV curves revealed a reversible redox reaction at 3.5 V to 4.0 V (oxidation) and 2.6 V to 3.4 V (reduction).

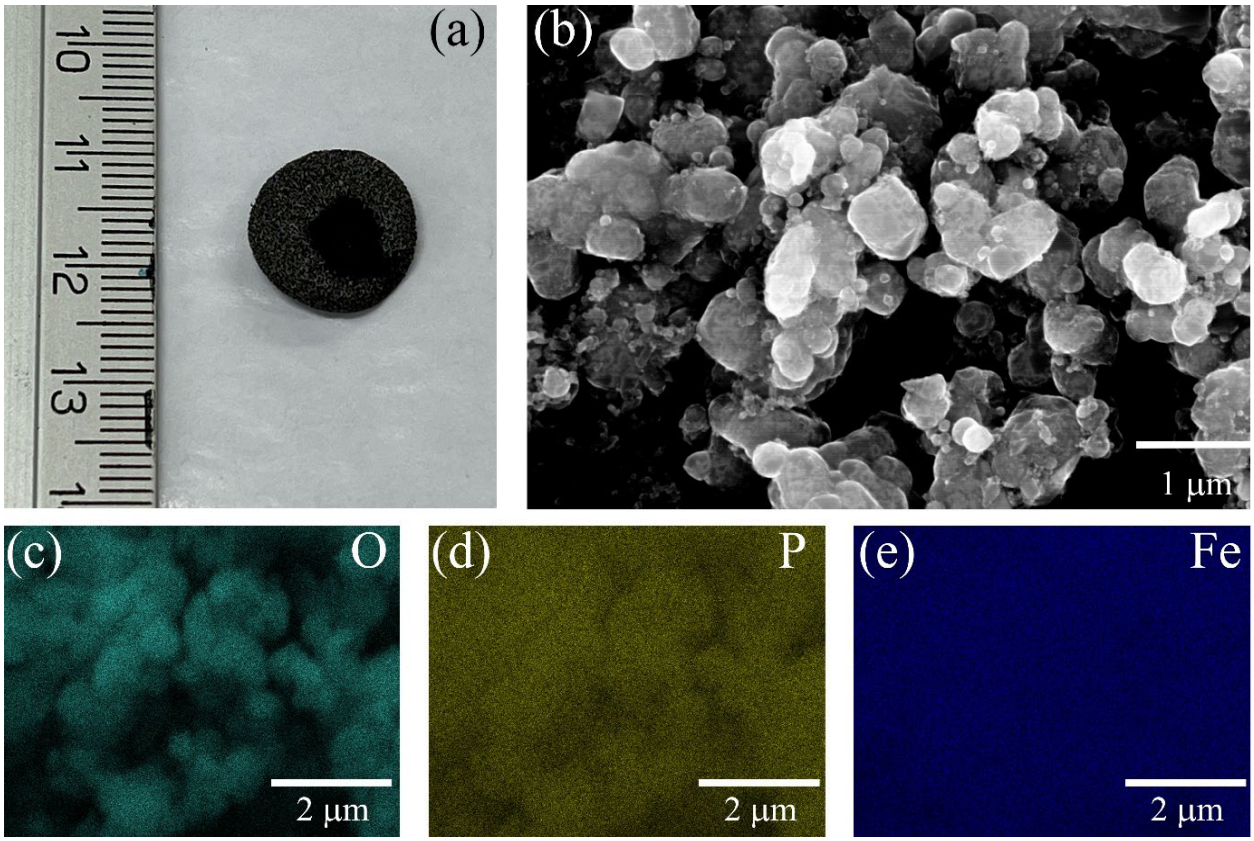

Figure 3. (a) Photograph of the LFP on graphene foam, (b) SEM image of the LFP on the graphene foam, (c-e) EDX elemental distribution maps for oxygen, phosphorus and iron, respectively.

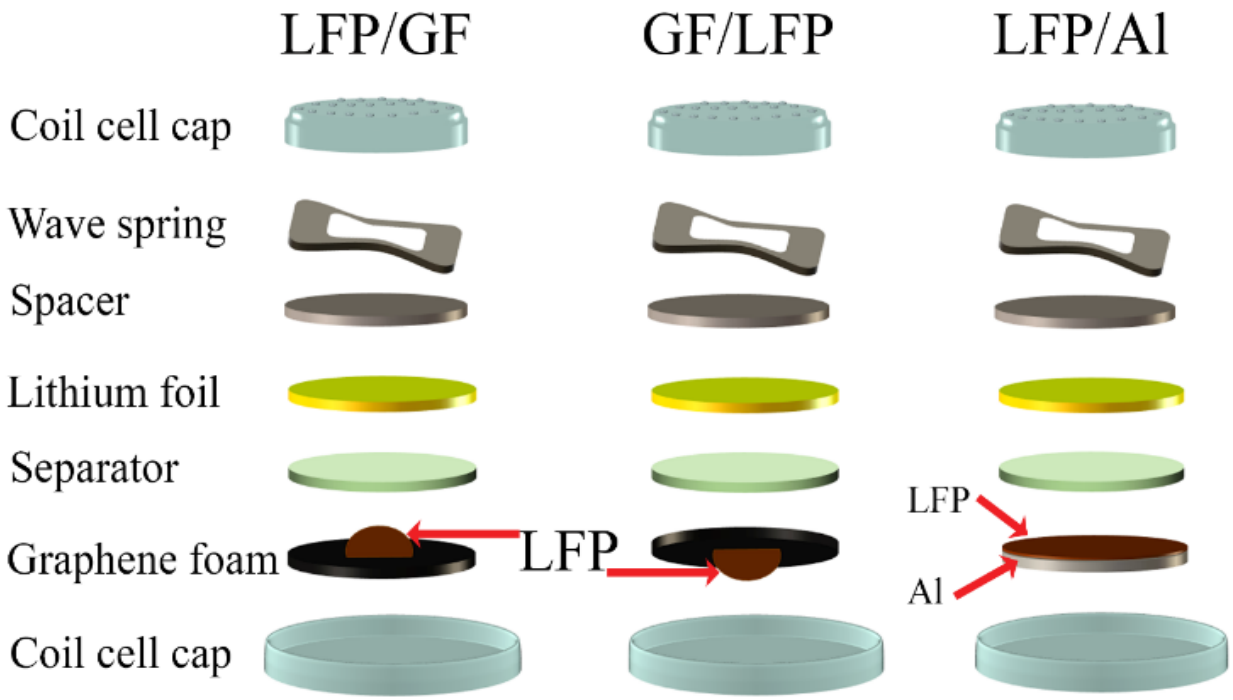

Figure 4. Three types of coin cell assemblies. (Left) The LFP between the separator sheet and the graphene foam (LFP/GF), (Middle) The graphene foam between the separator sheet and the LFP (GF/LFP), and (Right) The LFP between the separator sheet and the aluminum foil (LFP/Al).

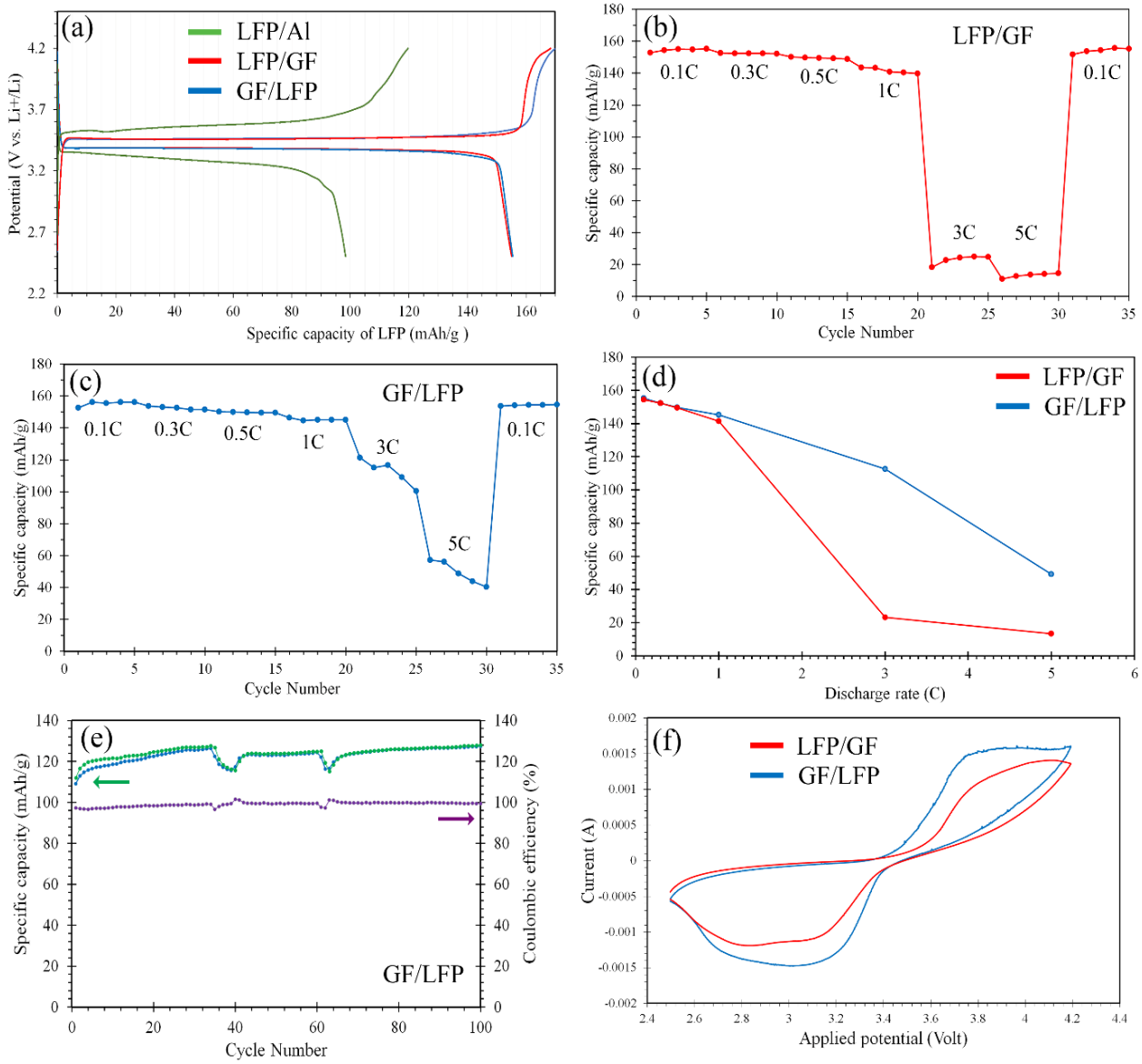

Figure 5. (a) Charge and discharge curve of LFP/Al (green), LFP/GF (red) and GF/LFP (blue) at current density of 0.1C. (b-c) Rate capabilities of LFP/GF and GF/LFP, respectively, at 0.1C-5C, (d) Relationship between the average specific capacity and the discharge rate of LFP/GF (red) and GF/LFP (blue), (e) Coulombic efficiency (purple) and cycling performance of charge (green) and discharge (blue) of GF/LFP at current density of 3C, and (f) Cyclic voltammetry curves of LFP/GF (red) and GF/LFP (blue) at scan rate of 1 mV·s^{-1}.

Figure 6(a) displays EIS of GF/LFP and LFP/GF which are fitted by a basis of the equivalent circuit as shown in the inset. The R_s, R_{ct}, CPE and Z_w, represent ohmic resistance, charge transfer resistance, capacitance of double layer and Li^+ migration related Warburg resistance, respectively [29]. Table 1 shows ohmic resistance and charge transfer resistance of GF/LFP and LFP/GF. The ohmic resistance and charge transfer resistance of GF/LFP was obviously lower than those of LFP/GF resulting in the specific capacity of GF/LFP was greater than that of LFP/GF at high current density.

At the low-frequency straight-line region (Warburg region), the diffusion coefficients of Li+ (D) of GF/LFP and LFP/GF were calculated using the following Equation [30].

$$D = \frac{R^2T^2}{2A^2n^4F^4C_{Li^+}^2\sigma^2} \quad (1)$$

where R, T, A, n, F, C_{Li+} and σ represent the gas constant, absolute temperature, surface area of the electrode, number of electron transfer, Faraday's constant, concentration of Li^+ and Warburg factor, respectively. The Warburg factors are calculated from the slopes of the graph between the real resistance and the inverse square root of angular frequency. Figure 6(b) reveals the Warburg factors of the GF/LFP and LFP/GF were 2.63 Ω s$^{-1/2}$ and 7.94 Ω s$^{-1/2}$, respectively. Therefore, the diffusion coefficients of Li^+ of GF/LFP is 9.1 times higher than that of LFP/GF.

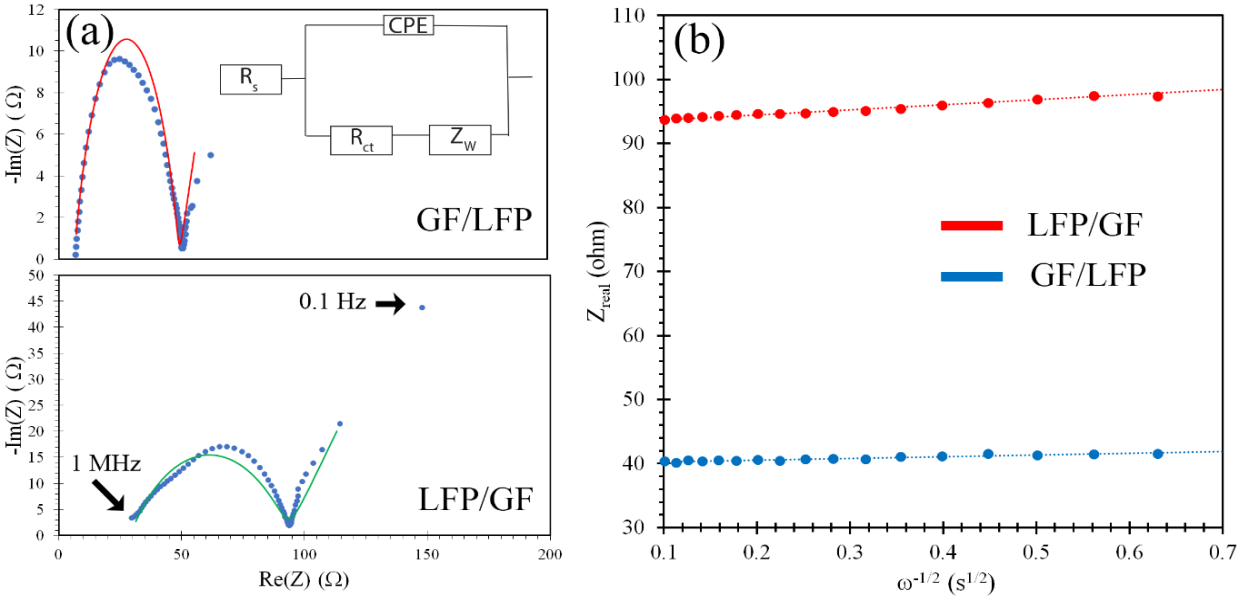

Figure 6. (a) Nyquist plots of GF/LFP and LFP/GF. The inset presents an equivalent circuit for fitting of the experimental data, and (b) Fitting curves of real resistance and inverse square root of angular frequency for GF/LFP and LFP/GF.

Table 1. ohmic resistance (Rs) and charge transfer resistance (Rct) of GF/LFP and LFP/GF.

Name	R_s (ohm)	R_{ct} (ohm)
GF/LFP	5.081	34.19
LFP/GF	28.96	64.31

4. Conclusions

We have demonstrated a method to improve the specific capacity of lithium iron phosphate battery by increasing the surface area, and electrical conductivity of the cathode electrode using the graphene foam. The results showed that the utilization of the graphene foam as the current collector can increase the specific capacity due to the high surface area and great electrical conductivity of the graphene foam. In addition, the presence of graphene foam between electrolyte and LFP can increase the transfer rate of ions at high current density due to the increment of diffusion coefficients of Li^+ and the reduction of ohmic resistance and charge transfer resistance.

Acknowledgements

This work was supported by the Thailand Science Research and Innovation Fundamental Fund fiscal year 2023, and Thammasat University Research Fund, Contract No. TUFT 7/2564, and Thammasat University Research Unit in Synthesis and Applications of Graphene.

References

[1] B. Scrosati, and J. Garche, "Lithium batteries: Status, prospects and future," *Journal of Power Sources*, vol. 195, pp. 2419-2430, 2010.

[2] A. K. Padhi, K. S. Nanjundaswamy, and J. B. Goodenough, "Phospho-olivines as Positive-Electrode materials for rechargeable Lithium batteries," *Journal of The Electrochemical Society*, vol. 144, pp. 1188-1194, 1997.

[3] J. M. Tarascon, and M. Armand, "Issues and challenges facing rechargeable lithium batteries," *Nature*, vol. 414, pp. 359-367, 2001.

[4] H. Raj, and A. Sil, "Effect of carbon coating on electrochemical performance of $LiFePO_4$ cathode material for Li-ion battery," *Ionics*, vol. 24, no. 26, pp. 2543-2553, 2018.

[5] J. F. Ni, H. H. Zhou, J. T. Chen, and X. X. Zhang, "$LiFePO_4$ doped with ions prepared by co-precipitation method," *Materials Letters*, vol. 59, pp. 2361-2365, 2005.

[6] Z. Tian, S. Liu, F. Ye, S. Yao, Z. Zhou, and S. Wang, "Synthesis and characterization of $LiFePO_4$ electrode materials coated by graphene," *Applied Surface Science*, vol. 305, pp. 427-432, 2014.

[7] H. Ji, L. Zhang, M. T. Pettes, H. Li, S. Chen, L. Shi, R. Piner, and R. S. Ruoff, "Ultrathin graphite foam: A Three-dimensional conductive network for battery electrodes," *Nano Letters*, vol. 12, pp. 2446-2451, 2012.

[8] A. K. Geim, and K. S. Novoselov, "The rise of graphene," *Nature Materials*, vol. 6, pp. 183-191, 2007.

[9] A. A. Balandin, S. Ghosh, W. Bao, I. Calizo, D. Teweldebrhan, F. Miao, and C. N. Lau, "Superior thermal conductivity of single-layer graphene," *Nano Letters*, vol. 8, pp. 902-907, 2008.

[10] T. Ohta, A. Bostwick, J. L. McChesney, T. Seyller, K. Horn, and E. Rotenberg, "Interlayer interaction and electronic screening in multilayer graphene investigated with angle-resolved photo-emission spectroscopy," *Physical Review Letters*, vol. 98, pp. 206802, 2007.

[11] A. Ruammaitree, H. Nakahara, K. Akimoto, K. Soda, and Y. Saito, "Determination of non-uniform graphene thickness on SiC (0001) by X-ray diffraction," *Applied Surface Science*, vol. 282, pp. 297-301, 2013.

[12] K. V. Emtsev, F. Speck, Th. Seyller, and L. Ley, "Interaction, growth, and ordering of epitaxial graphene on SiC{0001} surfaces:

A comparative photoelectron spectroscopy study," *Physical Review B*, vol. 77, p. 155303, 2008.

[13] L. Zhou, Z. Yang, J. Yang, Y. Wu, and D. Wei, "Facile syntheses of 3-dimension graphene aerogel and nanowalls with high specific surface areas," *Chemical Physics Letters*, vol. 677, pp. 7-12, 2017.

[14] I. A. Ovid'ko, "Mechanical properties of graphene," *Reviews on Advanced Materials Science*, vol. 34, 1-11, 2013.

[15] A. Ruammaitree, H. Nakahara, and Y. Saito, "Growth of protrusive graphene rings on Siterminated 6H–SiC (0001)," *Surface and Interface Analysis*, vol. 46, pp. 1156-1159, 2014.

[16] A. Ruammaitree, H. Nakahara, and Y. Saito, "Growth of non-concentric graphene ring on 6H-SiC (0001) surface," *Applied Surface Science*, vol. 307, pp. 136-141, 2014.

[17] H. Hu, A. Ruammaitree, H. Nakahara, K. Asaka, and Y. Saito, "Few-layer epitaxial graphene with large domains on C-terminated 6H-SiC," *Surface and Interface Analysis*, vol. 44, pp. 793-796, 2012.

[18] P. Surinlert, P. Kokmatb, and A. Ruammaitree, "Growth of turbostratic stacked graphene using waste ferric chloride solution as a feedstock," *RSC Advances*, vol. 12, pp. 25048-25053, 2022.

[19] P. Kokmat, P. Surinlert, and A. Ruammaitree, "Growth of high-purity and high-quality turbostratic graphene with different interlayer spacings," *ACS Omega*, vol. 8, pp. 4010-4018, 2023.

[20] A. Ruammaitree, D. Phokharatkul, and A. Wisitsoraat, "Surface hardening of stainless steel by coating graphene using thermal chemical vapor deposition," *Solid State Phenomena*, vol 283, pp. 173-178, 2018.

[21] P. Kokmat, N. Donnuea, N. Nuntawong, A. Wisitsoraat, and A. Ruammaitree, "Effect of acetic acid pre-treatment on the growth temperature of graphene on copper by thermal chemical vapor deposition," *IOP Conference Series: Materials Science and Engineering*, vol. 526, p. 012008, 2019.

[22] J. Oh, J. Lee, Y. Jeon, S. Park, J. M. Kim, T. Hwang, and Y. Piao, "Melamine foam-derived n-doped carbon framework and graphene-supported $LiFePO_4$ composite for high performance lithium-ion battery cathode material," *ACS Sustainable Chemistry & Engineering*, vol. 7, pp. 306-314, 2019.

[23] M. J. Matthews, and M. A. Pimenta, "Origin of dispersive effects of the Raman D band in carbon materials," *Physical review B*, vol. 59, pp. R6585- R6588, 1999.

[24] Y. L. Liu, C. C. Yu, C. Y. Fang, H. L. Chen, C. W. Chen, C. C. Kuo, C. K. Chang, L. C. Chen, and K. H. Chen, "Using optical anisotropy as a quality factor to rapidly characterize structural qualities of large-area graphene films," *Analytical Chemistry*, vol. 85, pp. 1605-1614, 2013.

[25] M. A. Pimenta, G. Dresselhaus, M. S. Dresselhaus, L. G. Cancado, A. Jorio, and R. Saito, "Studying disorder in graphite-based systems by Raman spectroscopy," *Physical Chemistry Chemical Physics*, vol. 9, pp. 1276-1291, 2007.

[26] C. Cong, T. Yu, R. Saito, G. F. Dresselhaus, and M. S. Dresselhaus, "Second-order overtone and combination raman modes of graphene layers in the range of 1690-2150 cm^{-1}," *ACS Nano*, vol. 5, pp. 1600-1605, 2011.

[27] R. Rao, R. Podila, R. Tsuchikawa, J. Katoch, D. Tishler, A. M. Rao, and M. Ishigami, "Effects of layer stacking on the combination Raman modes in Graphene," ACS nano, vol. 5, pp. 1594-1599, 2011.

[28] B. M. Goh, Y. Wang, M. V. Reddy, Y. L. Ding, L. Lu, C. Bunker, and K. P. Loh, "Filling the voids of graphene foam with graphene "Eggshell" for improved lithium-ion storage," *ACS Applied Materials & Interfaces*, vol. 6, pp. 9835-9841, 2014.

[29] J. Lu, X. Tian, Y. Zhou, Y. Zhu, Z. Tang, B. Ma, G. Wu, T. Jiang, X Tu, and G. Z. Chen, "A novel "holey-LFP/graphene/ holey-LFP" sandwich nanostructure with significantly improved rate capability for lithium storage", *Electrochimica Acta*, vol. 320, p. 134566, 2019.

[30] G. Luo, Y. Gu, Y. Liu, Z. Chen, Y. Huo, F. Wu, Y. Mai, X. Dai, and Y. Deng, "Electrochemical performance of in situ $LiFePO_4$ modifed by N-doped graphene for Li-ion batteries," *Ceramics International,* vol. 47, pp. 11332-11339, 2021.